Enhanced coupling of light from organic light emitting diodes using nanoporous films

H. J. Peng, Y. L. Ho, X. J. Yu, and H. S. Kwok
Center for Display Research, Department of Electrical and Electronic Engineering, Hong Kong University of Science and Technology, Clear Water Bay, Hong Kong, People's Republic of China

(Received 9 February 2004; accepted 30 April 2004)

We have demonstrated an approach to enhance the light extraction efficiency for organic light emitting diode (OLED). Nanoporous alumina film was used to modify the optical wave propagation and coupling of light from the OLED. Experimental results showed an increase of over 50% in the coupling efficiency of the nanoporous device, without affecting the electrical properties of the OLED. Effective medium theory can be used to model the optical properties of the nanoporous media and simulated the optical characteristics of the OLED successfully. © *2004 American Institute of Physics*. [DOI: 10.1063/1.1765859]

I. INTRODUCTION

The external quantum efficiency η_{ex} of organic light emitting diodes (OLED) is a product of the internal quantum efficiency η_{QE} and the optical out-coupling efficiency $\eta_{coupling}$.[1] The internal quantum efficiency is mainly affected by the nonradiative recombination loss and the singlet-triplet branching ratio. Most OLED materials have small nonradiative loss. Additionally, the application of phosphorescent emitting materials has been reported to overcome the singlet-triplet branching problem. Experimentally, it is possible to produce an internal quantum efficiency as high as 87%, which is very close to the theoretical limitation.[2]

On the other and, the coupling efficiency remains low. According to Greenham, Friend, and Bradley,[3] the coupling efficiency is given by

$$\eta_{coupling} = \frac{1}{\xi n^2},$$

where n is the refractive index and ξ is a constant that depends on the dipole alignment and the geometry of the OLED device. For most OLED materials, n is about 1.8.[3] Taking a value of 2 for ξ, then only about 20% of the generated light is coupled out. Physically most of the light is emitted into the waveguiding modes in the substrate and organic/indium tin oxide (ITO) layers. Therefore, the coupling efficiency is a major hurdle for achieving high efficiency devices.

A major limit to the coupling efficiency is total internal reflection (TIR). For the typical OLED structure, TIR can occur at the OLED substrate interface as well as the substrate/air interface. Several attempts have been made to enhance forward scattering at the latter interface. Yamasaki, Sumioka, and Tsutsui reported a periodic patterning of the substrate surface with a monolayer of silica microsphere.[4] Madigan, Lu, and Strum altered the geometry of the substrate to enhance the surface emission.[5] A factor of 3 enhancement was obtained. Möller and Forrest fabricated a microlens array on the substrate backside and increased $\eta_{coupling}$ by a factor of 1.5.[6] Matterson *et al.* demonstrated that through the use of corrugated microstructures, light could be coupled out by Bragg scattering. The corrugated light-emitting diode had two-times the efficiency as compared with an uncorrugated device.[7] Similar idea was also applied by Hobson *et al.* to recover the power lost to the surface plasmon modes.[8] Very recently, Lee *et al.* introduced a nano-patterned photonic crystal into the glass substrate to improve the coupling efficiency.[9] An enhancement factor of 1.5 over viewing angle of ±40° was achieved. Tsutsui *et al.* placed a low index aerogel material ($n \sim 1.01-1.10$) between the ITO layer and glass substrate to reduce the waveguide modes and achieved coupling enhancement of a factor of 1.8.[10]

In this paper we present a technique of using self-organized nanoporous anodic aluminium oxide (AAO) to improve the coupling efficiency in an OLED. It is well known that AAO is highly porous with a wide pore size in the nanometer range.[11,12] The nanoporous AAO is formed through a simple electrochemical process and then transferred to glass substrate through lamination. Organic light emitting devices were fabricated on the nanoporous substrates and were found to produce more than 50% enhancement of $\eta_{coupling}$.

II. SAMPLE PREPARATION

The basic idea is to use anodized alumina as the substrate to reduce light guiding in the OLED. Since the anodized surface is always very rough and not suitable for growing OLED, we tried to use the backside of the AAO film for growing the OLED. The process for fabricating the nanoporous substrate is as follows. First, an aluminium layer ($\sim 2\mu$m) was produced by rf sputtering on a glass substrate covered with a thin titanium film ($\sim$50 nm). Here, the titanium film was used both as a conductive layer to facilitate anodization of the aluminium metal as well as being a sacrificial layer for AAO film separation as discussed below. Aluminum anodization was performed in a 0.3M phosphoric acid solution at 5 °C under dc current. A platinum sheet was used as the cathode. The dc voltage was set at 150 V to obtain a large pore diameter and cell size. The anodic current density was found to be constant during the anodising process and went to zero when anodization of the aluminium

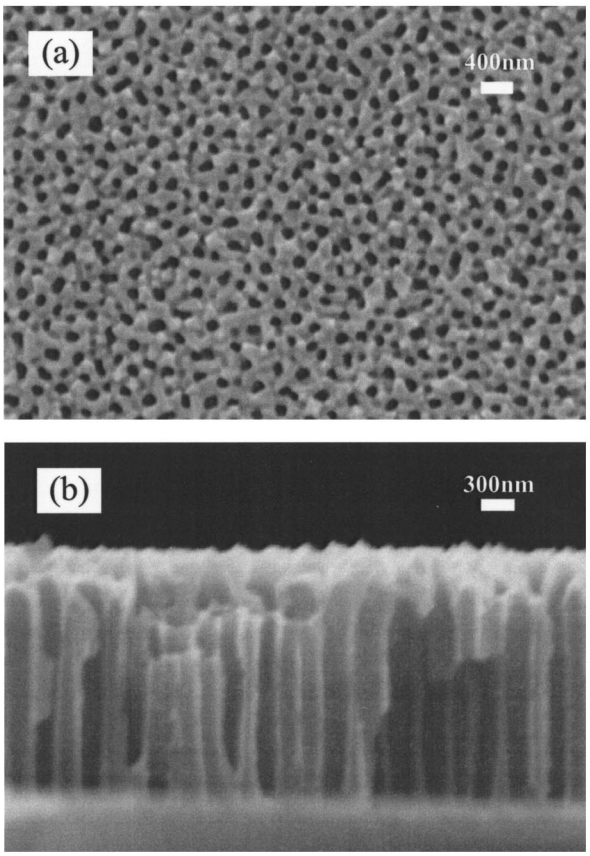

FIG. 1. SEM micrograph of the porous AAO films. (a) Top view of the sample before pore extension and (b) side-view of the sample after pore extension in a 5 wt% H_3PO_4 solution.

film was complete. After the initial pore formation, the pore diameter was extended relative to the pore spacing by using a 5 wt% H_3PO_4 solution.

After the AAO film was made, it was then transferred to a transparent substrate. It was achieved by laminating a transparent flexible film onto the AAO film and then attaching the entire film to a glass sheet using UV epoxy. The lamination process was performed very carefully to avoid air bubble inside. The sample was then immersed in H_2O_2 solution at 30 °C to etch away the sacrificial titanium film. The teching process was found to have no effect on the AAO layer. Thus a smooth surface, consisting of the backside of the original AAO film, was obtained. This surface is smooth due to the etching of the sacrificial titanium layer. This guarantees that a large area OLED device can be fabricated without discontinuities.

Figure 1 shows the scanning electron microscopy images of the microstructure of the AAO film before and after pore extension. The AAO film has a honeycomb structure with straight and parallel channels characterized by a closed packed array of columnar hexagonal cells, each containing a central pore. The pore size is 150–200 nm before extension and extended to ~300 nm after this processing step. The cell size is around 400–450 nm. The top view SEM pictures show the pore configuration of the sample is randomly aligned. It has been reported that ideally ordered AAOs could be obtained using master molding method[13] or by a two-step anodization method.[14] The optical transmittance of the anodic porous film on the glass substrate is an important parameter in making devices for optoelectronic application.

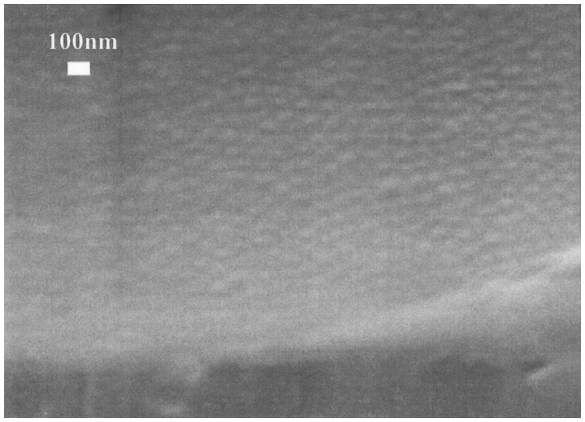

FIG. 2. SEM micrograph of the backside of AAO films after film transfer. The continuous layer is the barrier layer formed during anodization.

Figure 2 shows the AAO film after the film separation step. It is essentially the backside of the AAO film. It is noticed that this film is smooth and is suitable for OLED deposition. Figure 3 shows the transmittance spectra of the nanoporous substrates using the AAO with and without pore extension. As the aluminium is completely converted into oxide, the average transmittance of the anodic oxide film in visible range reaches ~95% before the pore extension. After the pore extension process, however, the transmittance is lowered, especially in the short wavelength region. That indicates the light scattering becomes stronger in the visible and blue region.

In order to find out whether the nanoporous substrate could increase the out-coupling efficiency, we first investigated the photoluminescence (PL) characteristics of organic emitting film on the formed substrates. An *N*,*N*′-diphenyl-*N*,*N*′ bis(3-methylpheny-l, 1'-biphenyl-4,4'-diamine (TPD) +5% rubrene film was deposited on the nanoporous substrate and a control sample was deposited on a bare glass substrate. The PL measurement of the two samples was carried out under identical conditions. Excitation was provided by the 450 nm line of argon-ion laser and the PL emission was detected by a PhotoResearch PR705 SpectraScan spectrophotometer. The angular distribution of PL emission was

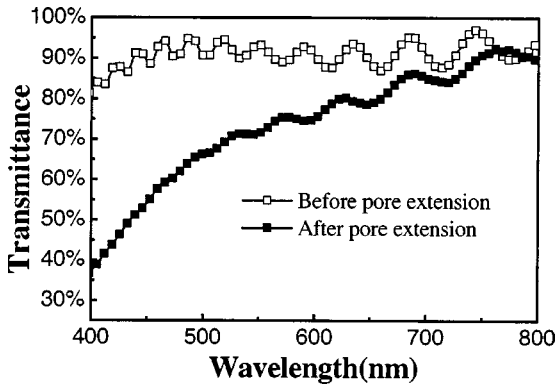

FIG. 3. Transmittance of the AAO films, (a) before the pore extension and (b) after pore extension.

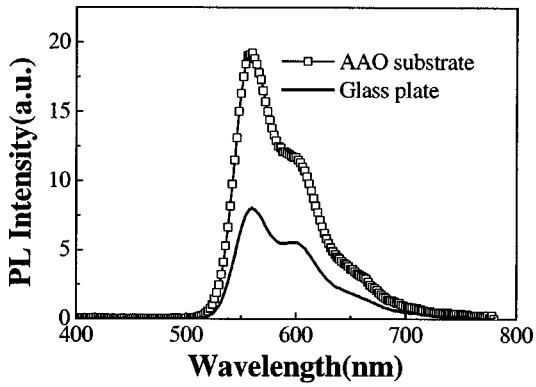

FIG. 4. Photoluminescence (PL) spectra in the normal direction of the TPD+5% rubrene film on nanoporous substrate and bare glass sheet.

also measured. Figure 4 shows the comparison of the PL spectra of the two samples in the normal direction. It can be seen that the PL output of the AAO device at normal incidence is enhanced by a factor of 2 over the control sample. Figure 5 shows the angular distribution of the PL intensity. Evidently, the PL signal from the AAO sample has a wider angular distribution. In fact, it peaks at an angle of near 60° instead of in the normal direction. Obviously some sort of microcavity effect is present enhancing the emission at these angles. In order to evaluate quantitatively the total PL signal from both samples, the total emission is calculated according to the equation

$$L = 2\pi A \int_0^{\pi/2} I(\theta)\sin\,\theta d\theta \approx 2\pi A \sum_n I(\theta_n)\sin\,\theta_n \Delta\theta, \quad (1)$$

where $I(\theta_n)$ is the measured radiant intensity at the viewing angle θ_n, A is the emitting area, and the emission is assumed to be azimuthally symmetrical. The calculated integrated PL signal from the nanoporous sample is about three times larger than the control. Since the only difference between the two cases is the presence of the AAO film underneath the TPD emitting layer, it is concluded that the increased PL signal is due to less light guiding effect. The PL measurement result indeed indicated that the application of the nanoporous AAO could improve the light extraction efficiency.

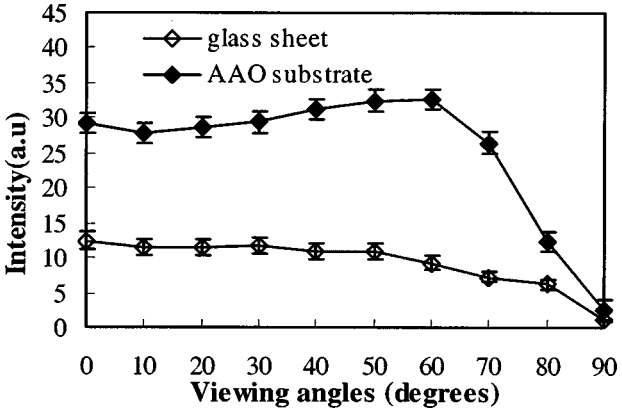

FIG. 5. Radiant intensity angular distribution of PL emission.

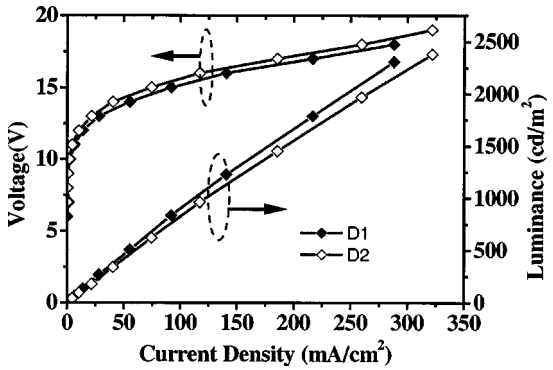

FIG. 6. *J-L-V* curves of OLED on nanoporous substrate (D1) and a control device on bare glass substrate (D2). The OLED is formed as Pt/CuPc/TPD/TPD+5wt% ruberene/Alq/LiF/Al multilayer structure.

III. OLED DEVICES

In order to examine the effects of the AAO substrate to electroluminescent (EL) devices, we fabricated OLED devices on the smooth nanoporous substrate. We used 100 Å Pt film directly deposited on the AAO film as the anode. This Pt film is only partially transparent and it is expected that some light will be lost. The device structure consists of a hole injection layer of copper (II) phthalocyanine (CuPc), a hole transport layer of TPD, an emitting layer of TPD+5 wt% rubrene, and an electron transport layer (ETL) of tris-8-hydroxyquinoline aluminium Alq3, followed by LiF/Al as the reflective cathode. This is a conventional OLED structure except for the use of Pt as the anode instead of the usual ITO. All films were deposited in a high vacuum evaporation system, with a background pressure of 1×10^{-6} Torr. The active emitting area was defined to be $\sim1.5\times1.5$ mm^2 using a shadow mask during cathode position. A control device was also fabricated with the same OLED structure except that the substrate was just bare ITO glass without the nanoporsous AAO film. EL intensity of both devices was measured using a PR650 SpectraScan spectrophotometer. Current-voltage (*J-V*) characteristics were measured using an Advantest R6145 dc voltage current source and Fluke 45 Dual Display multimeter. All the measurements were conducted in air ambient.

The luminance (L)–current-density (J)– voltage (V) characteristics of the OLED on the nanoporous substrate, together with the control device, are summarized in Fig. 6. The *J-V* performances of two devices are almost the same because the film thickness and layer structure are identical. The slight discrepancy between the two *J-V* curves is believed to be due to the different substrate morphology. The luminance current efficiency η of the devices can be obtained from the *L-J* dependence in Fig. 6. The η values are $\sim$1.0 cd/A for device on nanoporous substrate and $\sim$0.9 cd/A for the control devices in the normal direction. Thus it seems that there is not much difference between the two samples. However, the situation is quite different if the angular distribution is taken into consideration.

Normally, emission from the OLED is Lambertian. However, it has also been shown by rigorous theoretical modeling that the emission profile of the conventional device is dependent on both the thicknesses of the organic and ITO

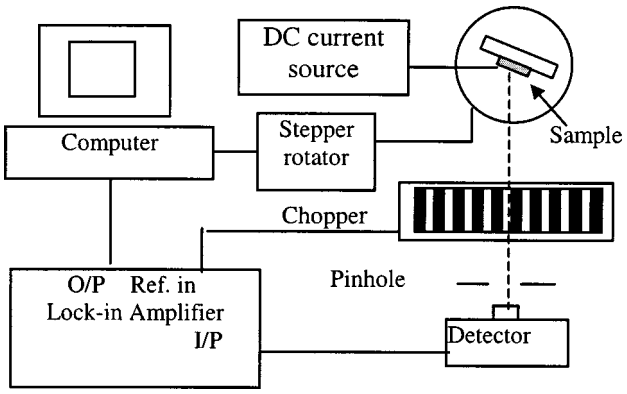

FIG. 7. Schematic diagram of the setup for the EL device angular distribution measurement.

layers due to a microcavity effect.[15] For devices with substrate modification, the emission profiles have been demonstrated to be quite different from Lambertain.[5,6] In this case, it is important to measure the far-field emission profile of the devices for total photon flux estimation.

Figure 7 shows the measurement systems to test the angular distribution profile. The sample was fixed at a rotating stage. The distance between the center position and photodector was 20 cm so that the device could be treated as a point source. The device was driven by a Keithley constant current source. The measurement was performed automatically using a LABVIEW program. The normalized distribution profiles of nanoporous device and conventional one are given in Fig. 8. Both the nanoporous device and the control device show non-Lambertian behavior. When the viewing angle is larger than 20°, the control device had intensities smaller than cosine lambertian. On the other hand, the nanoporous device had intensities higher than Lambertian. The EL spectra of both devices measured at different viewing angles are presented in Fig. 9. For the control device, the full width at half maximum (FWHM) of the spectra decreases from 56 nm at 0° to 48 nm at 70° while the peak wavelengh remains almost identical at 556–560 nm. For the nanoporous device, the FWHM decreases with larger viewing angle from 68 nm at 0° to 52 nm at 70°, and the peak wavelength shifts

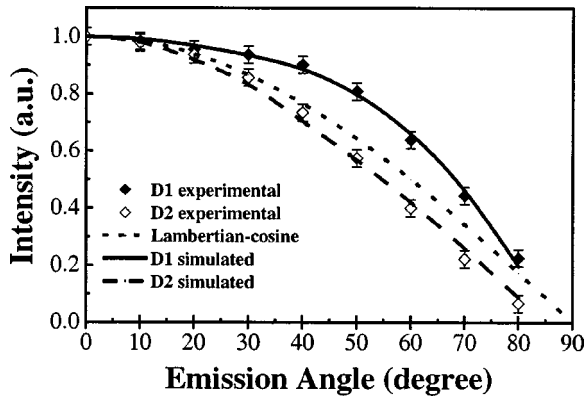

FIG. 8. Measured angular distribution profiles of the nanoporous device (filled diamonds) and the control device (open diamonds) and simulated emission pattern for both devices. The dotted line corresponds to the cosine Lambertian behavior for reference.

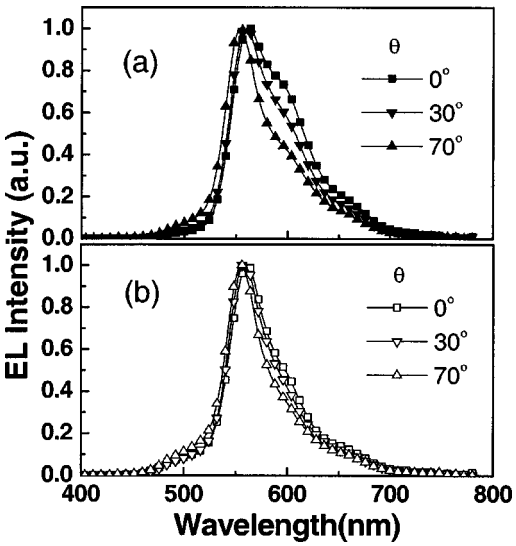

FIG. 9. Normalized EL spectra measured at different viewing angles of the nanoporous device (a) and the control device (b).

from 544 nm at 0° to 536 nm at 70°. The variation of the photodetector output signal due to the spectrum change was carefully tested and found to be small enough, less than 3%, to be ignored. The total radiant flux L of the light emission extracted from an OLED surface can be obtained by performing the integration as shown in Eq. (1). Integrating the light flux in the forward 160° cone, the nanoporous device is found to emit 50% more photons than the conventional device. This is quite a significant improvement.

IV. THEORETICAL CALCULATION OF THE ANGULAR DISTRIBUTION

In order to understand the enhancement mechanism, we simulated the emission characteristics of the OLEDs, either the control one or that on the nanoporous substrate, using a rigorous classical electrodynamic methods based on Green function and a plane wave propagation method.[16,17] Figure 10 shows the schematic diagram of the device structure for modeling. First, we assumed the recombining excitons in the emission layer can be represented as electric oscillating dipoles. Then the device emission characteristics can be obtained by calculating the intensity distribution of the electromagnetic field generated from oscillating dipoles embedded in a planar stratified media. In an unbounded medium the dipole oscillation can be described by a electric Hertz vector $\vec{\Pi}^{(e)}$. This Hertz vector satisfies the vector Helmholtz equation as:[18]

$$(\nabla^2 + k^2)\vec{\Pi}^{(e)} = -4\pi\vec{P}_0\delta(\vec{r}), \tag{2}$$

where k is the wave vector, $\vec{P}_0$ is vector dipole moment, and δ is the delta function. The solution of the equation gives the dipole radiation, which is actually a spherical wave. The Fourier spectrum of the wave field in the in-plane wave vector $k//$ space shows it can be represented as a superposition of plane and evanescent waves. Meanwhile, the vector dipole moment can be decomposed in the three orthogonal configurations to divide the dipole radiation field into s (TE) and

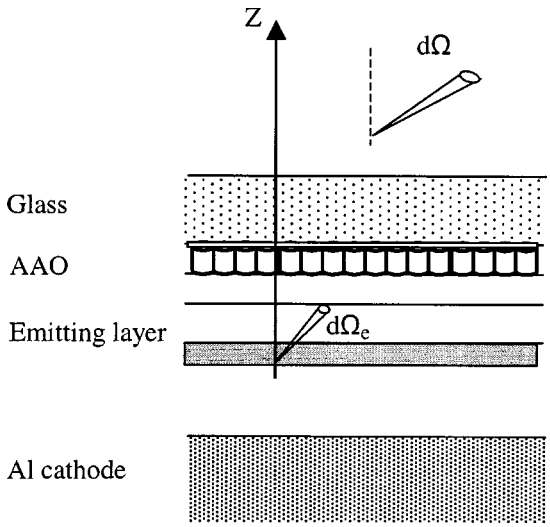

FIG. 10. Schematic diagram of layered structure of OLED on nanoporous AAO substrate for optical simulation. The solid angle changes when light propagates from layer to out medium due to different refractive indices.

p (TM) polarized components. Upon propagating through the multiplayer structure, these polarized plane and evanescent waves are subject to reflections, transmission, and absorption, which can be calculated, without any approximation, according to the Fresnel equations for multilayer structures. With the transfer-matrix method, we can therefore calculate the propagation of the source fields to the outside, including all interference effects. Finally, the far-field emission pattern (Poynting vector flux per unit solid angle) can be calculated with the following expression:

$$\frac{dP}{d\Omega} = |E_{\text{out}}|^2 \frac{n_0 {k_{z,0}}^2}{n_e {k_{z,e}}^2}, \tag{3}$$

where E_{out} is the calculated electrical field outside the OLED in terms of the total dipole radiation power, n is the refractive index, and k_z is the normal component of the wave vector, and the subscripts o and e denote the outside medium and emitting layer, respectively. In this calculation, the wavelength dipole oscillator strength and modification of the spontaneous radiative decay rate have also been taken into account.

In this model calculation, the optical constants of the various layers are important parameters for Fresnel coefficients calculation. For the anode and cathode layers and organic films, these parameters are measured using spectroscopic ellipsometry. For the nanoporous AAO film, we applied the effective medium theory (EMT) to obtain the optical constants. It has been reported that EMT can be used to model the propagation of waves in a media with corrugation with a characteristic dimension in the subwavelength region.[19] The formed nanoporous AAO is considered to be an array of circular rod with relative permittivity ε_2 (=1for air hole), immersed in a material of relative permittivity ε_1 (=2.72 for anodized alumina). So the effective permittivity ε can be expanded as a power series of the period-to-wavelength ratio α as given by

$$\varepsilon = \varepsilon_0 + \frac{\pi^2}{3}[f(1-f)(\varepsilon - \varepsilon_1)]^2 \alpha^2 + O(\alpha^4), \tag{4}$$

for TE polarization and

$$\varepsilon = \frac{1}{\alpha_0} + \frac{\pi^2}{3}\left[f(1-f)\frac{(\varepsilon_1 - \varepsilon_2)}{\varepsilon_1 \varepsilon_2} \right]^2 \frac{\varepsilon_0}{\alpha_0^3}\alpha^2 + O(\alpha^4), \tag{5}$$

for TM polarization, where $\varepsilon_0 = \varepsilon_2 f + (1-f)\varepsilon_1$ is the average relative permittivity and α_0 is the arithmetic average of the inverse relative permittivity, i.e., $\alpha_0 = f/\varepsilon_2 + (1-f)/\varepsilon_1$. For two given permittivities ε_2 and ε_1, the hole filling factor and the period of the corrugated structure, the porous AAO is modeled as a quarter-wave stack having effective permittivities of two polarization. The calculation shows that the effective refractive index $n(=\sqrt{\varepsilon})$ of the AAO film is $n=1.295$ for TE polarization and $n=1.15$ for TM polarization. With the obtained optical properties of the each layer, the far-field emission profiles of the devices were simulated using standard wave propagation calculations.[16,17] The simulation results for the distribution profiles are also given in Fig. 8. It is found that the theoretical calculation agrees with the experimental results quite well.

The light generated in the organic emitting layer travels through the organic layer, the transparent electrode, and the glass substrate before being extracted out into air. Due to refractive index mismatch, most of the light will be totally reflected internally inside the organic layer and glass substrate as waveguide modes. Because the organic layer is very thin, the guided mode intensity inside the organic layer is not strong and much of the light is guided inside the substrate.[20] In our experiment, the intensity enhancement of the normal direction is only 10%, less than that obtained using low index aerogel method. That is because the straight pores in the AAO film is not highly order, which deteriorates the enhancement. However, we believe there is still much room for improvement in the nanoporous structure. Further work will be undertaken on fabrication highly ordered nanoporous film and optimization of the cell size and pore diameter to obtain higher coupling efficiency enhancement.

V. CONCLUSION

In this paper, we have demonstrated a structure using nanoporous substrate for organic light emitting device to enhance the out-coupling efficiency. The self-organized, highly porous material with nanosize channels were obtained using the technique of anodic alumina oxidation together with a transfer process. That process enables a smooth surface to be available for OLED formation. Experimentally, 200% photoluminescence and 50% electroluminescence enhancement were realized from the device based on the formed nanoporous substrate. We have also successfully modeled the optical properties of the nanoporous film using the EMT and simulated the emission angular distribution of the devices. The theoretical calculations and the experimental results agree with each other very well, indicating that our explanation is valid. Finally, it is believed that larger enhancement in PL

and EL could be achieved by ordering the pore arrangement and optimizing the cell size and pore diameter.

ACKNOWLEDGMENT

This research was sponsored by Hong Kong SAR Research Grants Council.

[1]N. K. Patel, S. Cinà, and J. H. Burroughes, IEEE J. Sel. Top. Quantum Electron. **8**, 346 (2002).
[2]C. Adachi, M. A. Baldo, M. E. Thompson, and S. R. Forrest, J. Appl. Phys. **90**, 5048 (2001).
[3]N. C. Greenham, R. H. Friend, and D. D. C. Bradley, Adv. Mater. (Weinheim, Ger.) **6**, 491 (1994).
[4]T. Yamasaki, K. Sumioka, and T. Tsutsui, Appl. Phys. Lett. **76**, 1243 (2000).
[5]C. F. Madigan, M. H. Lu, and J. C. Strum, Appl. Phys. Lett. **76**, 1650 (2000).
[6]S. Möller and S. R. Forrest, J. Appl. Phys. **91**, 3324 (2002).
[7]B. J. Matterson, J. M. Lupton, A. F. Safonov, M. G. Salt, W. L. Barnes, and I. D. W. Samuel, Adv. Mater. (Weinheim, Ger.) **2**, 123 (2001).
[8]P. A. Hobson, S. Wedge, J. A. E. Wasey, I. Sage, and W. L. Barnes, Adv. Mater. (Weinheim, Ger.) **14**, 123 (2002).
[9]Y.-J. Lee, S.-H. Kim, J. Huh, G.-H. Kim, Y.-H. Lee, S.-H. Cho, Y.-C. Kim, and Y. R. Do, Appl. Phys. Lett. **82**, 3779 (2003).
[10]T. Tsutsui, M. Yahiro, H. Yokogawa, K. Kawano, and M. Yokoyama, Adv. Mater. (Weinheim, Ger.) **13**, 1149 (2001).
[11]H. Masuda and K. Fukuda, Science **268**, 1466 (1995).
[12]H. Masuda, F. Hasegawa, and S. Ono, J. Electrochem. Soc. **144**, L127 (1997).
[13]H. Asoh, K. Nishio, M. Nakao, T. Tamamura, and H. Masuda, J. Electrochem. Soc. **148**, B152 (2001).
[14]A.-P. Li, F. Müller, A. Birner, K. Nielsch, and U. Gösele, Adv. Mater. (Weinheim, Ger.) **11**, 483 (1999).
[15]T. Tsutsui and K. Yamamato, Proc. SPIE **3474**, 2 (1998).
[16]W. Lukosz, J. Opt. Soc. Am. **71**, 744 (1981).
[17]H. Benisty, R. Stanley, and M. Mayer, J. Opt. Soc. Am. B **15**, 1192 (1998).
[18]M. Born and E. Wolf, *Principles of Optics*, 7th ed. (Cambridge Univeristy Press, Cambridge 1999).
[19]P. Lalanne, Appl. Opt. **35**, 5369 (1996).
[20]M. H. Lu and J. C. Sturm, J. Appl. Phys. **91**, 595 (2002).